A Variational Ansatz for Taylorized Imaginary Time Evolution

Matthias Koch,* Oliver Schaudt, Georg Mogk, Thomas Mrziglod, Helmut Berg,
and Michael Edmund Beck

Read Online

ACCESS | Metrics & More | Article Recommendations

ABSTRACT: Being able to predict molecular properties and interactions is of utmost interest for academia as well as industry. But the vast complexity of strongly correlated molecular systems limits the performance of classical algorithms. In contrast, quantum computation has the potential to be a game changer in the field of molecular simulations. Despite the hope in quantum computation, the capabilities of current quantum computers are still insufficient for handling molecular systems of interest. In this paper, we propose a variational ansatz for today's noisy quantum computers to calculate the ground state with the help of imaginary time evolution. Although the imaginary time evolution operator is not unitary, it can be implemented on a quantum computer by a linear decomposition and subsequent Taylor series expansion. This has the advantage that only a set of shallow circuits needs to be computed on a quantum computer. The parallel nature of this algorithm can be exploited to speed-up simulations even further, if a privileged access to quantum computers is granted.
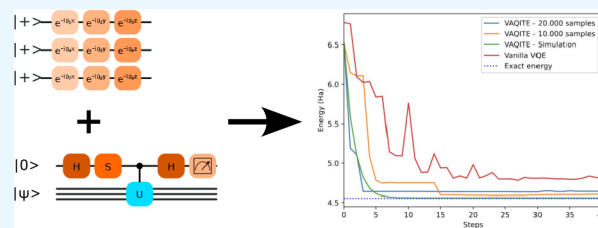
INTRODUCTION

When developing novel drugs, a detailed understanding of the active ingredient and the target is a must. To elucidate the mechanisms at work an interplay of demanding theoretical and experimental techniques is key. In spite of all that, brute-force high-throughput screening (HTS) is still the most prevalent technique for finding the next hit compounds. Just recently, computer-aided drug design is employed to increase the efficiency of HTS.[1−4] By preselecting promising candidates, the number of compounds necessary to screen is reduced. But theoretical simulations are often limited by the exorbitant high computational costs, in particular when strong electron correlation and/or multireference systems come into play. Accordingly, severe approximations are an absolute necessity even so they might falsify the results.[5] Nevertheless, the benefit of computational methods for drug discovery is immense. Instead of costly experiments, the interaction between novel compounds and a target protein can be simulated in-silico.[6−8] Here, quantum computation will have a disruptive force.[9] Fully error-corrected quantum computers come along with the promise of an exponential speed-up when simulating large molecular systems.[10] This would be a game-changer in the field of drug discovery. However, today's quantum hardware is not mature enough to directly run ground state calculations as for instance with the quantum phase estimation algorithm.[10−12] Not only is a much higher qubit-count needed for these, but also sophisticated error-correction is necessary when running deep quantum circuits.[13,14]

Therefore, a different approach is needed for the currently available imperfect quantum hardware. A common way to mitigate noise is with hybrid algorithms[15] consisting of parametrized quantum circuits (PQCs). The overlap between the PQC and the state of interest is assessed by a cost function, where some (or all) of the terms of the cost function are calculated on a quantum computer. The rotational angles are then updated according to a classical optimization routine. The advantage is that hybrid algorithms are shallow enough to run on current quantum hardware. A very popular example is the variational quantum eigensolver (VQE) for computing the ground state of a Hamiltonian.[16−19] But with increasing complexity of the Hamiltonian/PQC, the classical optimization of the PQC becomes more and more difficult. In particular the required number of measurements/optimization iterations to compensate the (exponentially) vanishing gradients might scale exponentially with the circuit depth and qubit count.[20,21]

Imaginary time evolution (ITE) on the other hand is a very powerful technique when calculating the ground state of large systems.[22,23] It has the advantage that it always converges to the ground state as excited states are exponentially suppressed with proceeding time.[24] Furthermore, ITE is the key ingredient of classical Quantum Monte Carlo (QMC) simulations, which allow economic and memory saving calculations of large molecules.[25,26] The idea of ITE is to substitute the time t with
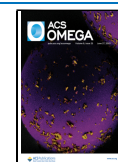
$-i\tau$ in the Schrödinger equation, where t and τ are real parameters. With the advent of quantum computing hardware, many studies investigate how quantum computation can be used to make QMC calculations more efficient.[27,28] The fact that the ITE operator $e^{-\mathbf{H}\tau}$ is not unitary (**H** is hermitian), and thus cannot be implemented directly on a quantum computer, is an obstacle. In literature this is addressed by three different techniques to realize ITE on quantum hardware: variational ITE (VITE),[24] probabilistic ITE (PITE),[29] and quantum ITE (QITE).[30]

VITE is a hybrid algorithm, which is based on the McLachlan's variational principle. It benefits from quantum computers when calculating expectation values. The main ingredient of this approach is the following expression

$$\delta \left\| \left(\frac{\partial}{\partial \tau} + \mathbf{H} - E_\tau \right) |\psi(\tau)\rangle \right\| = 0 \tag{1}$$

to progress $|\psi(\tau)\rangle$ toward the ground state. PITE on the other hand tries to solve this in a probabilistic manner by applying Grover's algorithm.[31,32] An ancilla qubit is used to apply the imaginary time-evolution operator onto the input state. If the measurement outcome of the ancilla qubit is $|0\rangle$, the state collapses to the desired time-evolved state. Lastly, QITE uses the fact that the Hamiltonian can be decomposed into partial Hamiltonians $\mathbf{h}[m]$ and a new hermitian operator $\mathbf{A}[m]$ is learned that minimizes the following term:

$$\left\| \frac{e^{-\Delta\tau\mathbf{h}[m]}|\psi_n\rangle}{\sqrt{\langle\psi_n|e^{-2\Delta\tau\mathbf{h}[m]}|\psi_n\rangle}} - e^{-i\Delta\tau\mathbf{A}_n[m]}|\psi_n\rangle \right\|^2 \tag{2}$$

STATE PREPARATION AND IMAGINARY TIME EVOLUTION

The approach discussed in this paper is based on similar ideas. In contrast to PITE and QITE, our algorithm relies on a parametrized circuit, similar to VQE, VITE, or matrix product states.[16,24,33] VITE uses McLachlan's variational principle to compute the updated rotational angles directly without any classical minimization procedure.[24] The algorithm proposed here utilizes classical optimization to find the next time evolved state by maximizing the overlap between $\langle\psi(\Theta_{n+1})|e^{-\tau\mathbf{H}}|\psi(\Theta_n)\rangle$ (for comparison purposes VQE minimizes the following equation $\langle\psi(\Theta)|\mathbf{H}|\psi(\Theta)\rangle$[16]). This ansatz is a mixture of VQE and VITE: We compute the ground state by time-evolution, but we still rely on classical optimization to find the next set of rotational angles defining the time-evolved state. To make $e^{-\mathbf{H}\tau}$ unitary we apply the Taylor approximation and measure the terms for the classical cost function with the help of the well-known Hadamard tests. We want to highlight that this algorithm is very resource-effective. Each term consists of a short PQC where only one qubit needs to be measured. The PQC for the ansatz state can be chosen in an efficient way to reduce the number of necessary Trotter steps to a minimum. First, a trivial ansatz is used, neglecting any c-not gates required to build entangled states (see Figure 1a). For this trivial ansatz, the state vector at time n is built by a set of rotations by $\Theta_{n,k,l}$ around the axis $\sigma_{p_{n,k,l}}$ with $p_{n,k,l} \in [1, x, y, z]$:

$$|\psi(\Theta_n)\rangle = \prod_k \otimes_l e^{-i\Theta_{n,k,l}\sigma_{p_{n,k,l}}}|+\rangle = \mathbf{U}_{\Theta_n}|+\rangle \tag{3}$$

The Hamiltonian describing our molecule (or optimization problem) is mapped onto the qubit space via the Parity
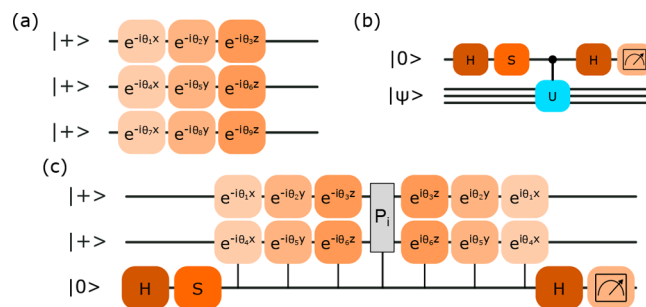
Figure 1. (a) Possible ansatz to build the molecular state. (b) Quantum circuit of a Hadamard test with an optional S-gate for extracting the imaginary instead of the real part. (c) Circuit which is executed to measure the real (without S-gate) or imaginary part (with S-gate) for the Pauli string P_i in eq 9.

transformation,[34] Jordan–Wigner transformation,[35] or Bravyi–Kitaev[36] transformation. A key ingredient is that the Hamiltonian operator is simplified by a linear decomposition. In the case of this work, a finite linear combination of Pauli operators was chosen: $\mathbf{H} = \sum_i^N \alpha_i \mathbf{P}_i$ with $\mathbf{P}_i = \otimes_m \sigma_{p_{i,m}}$ and $p_{i,m} \in [1, x, y, z]$. Accordingly the time evolution operator becomes $e^{-\tau\mathbf{H}} = e^{-\tau\sum_i^N \alpha_i \mathbf{P}_i}$. Here, we want to state again, this operator is nonunitary. We address this by applying a Taylor series expansion:

$$e^{-\tau\sum_i^N \alpha_i \mathbf{P}_i} = \sum_{k=0}^{N_{Taylor}=\infty} \frac{\tau^k}{k!} \left(\frac{\partial^k}{\partial\tau^k} e^{-\tau\sum_i^N \alpha_i \mathbf{P}_i} \right)_{\tau=0} \tag{4}$$

which, when considering the first order $N_{Taylor} = 1$, reduces to

$$e^{-\tau\sum_i^N \alpha_i \mathbf{P}_i} \approx \sum_{k=0}^{N_{Taylor}=1} \frac{\tau^k}{k!} \left(\frac{\partial^k}{\partial\tau^k} e^{-\tau\sum_i^N \alpha_i \mathbf{P}_i} \right)_{\tau=0} = 1 - \tau \sum_i^N \alpha_i \mathbf{P}_i \tag{5}$$

In contrast to the nonunitary exponential time-evolution operator, this truncated Taylor expanded version is not only unitary but also trivial to implement on gate-based quantum computers.

The path of the time evolution is treated as a maximization problem. In the case of a first order Taylor polynomial, the rotational angles Θ_{n+1} for the point in time $n + 1$ are found by maximizing the following term:

$$\left| \langle\psi(\Theta_{n+1})| \left(1 - \tau \sum_i^N \alpha_i \mathbf{P}_i \right) |\psi(\Theta_n)\rangle \right|^2 \tag{6}$$

where $|\Theta_n\rangle$ is considered as "the correct state" at time point n. As a consequence, its rotational angles Θ_n are not part of the optimization routine. Only the rotational angles Θ_{n+1} are varied when maximizing term 6. Subsequently, when computing $|\psi(\Theta_{n+2})\rangle$, $|\psi(\Theta_{n+1})\rangle$ will be the next "correct" state. In other words, this algorithm performs an incremental time evolution, where the rotational angles of the previous state are kept fixed while the angles of the successor are computed. The linear structure of the Taylor expansion allows us to write term 6 as

(a)

(b)
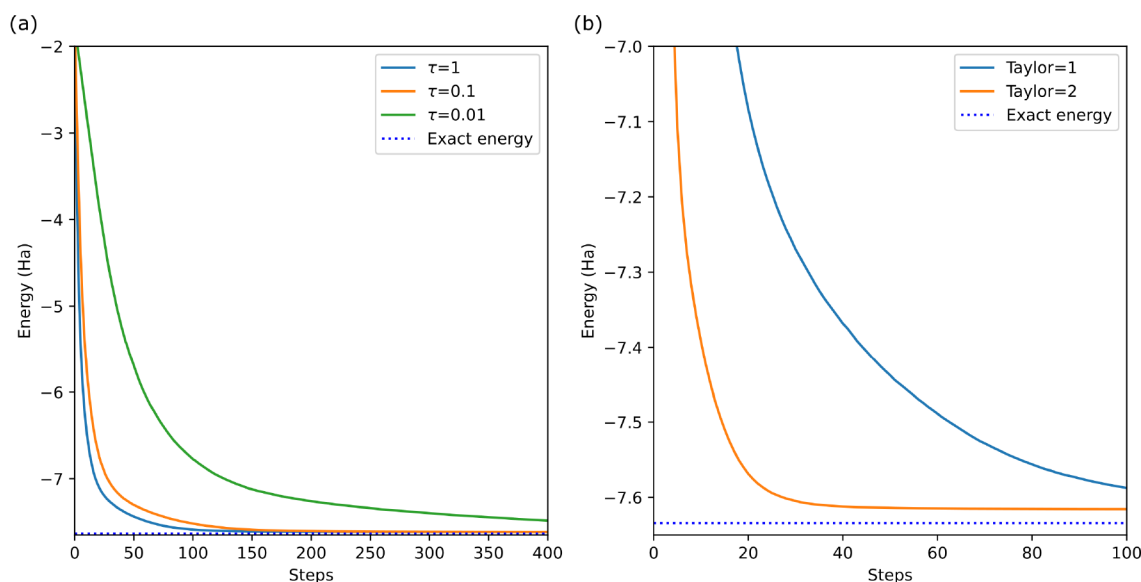
Figure 2. (a) First order Taylor expansion imaginary time evolution of LiH for different τ values. (b) Time evolution of LiH for two different Taylor expansion orders with $\tau = 1$ (compare to eq 4).

$$\left| \langle \psi(\Theta_{n+1}) | \left(1 - \tau \sum_i^N \alpha_i \mathbf{P}_i\right) | \psi(\Theta_n) \rangle \right|^2 = |\langle \psi(\Theta_{n+1}) | \psi(\Theta_n) \rangle|^2$$
$$- \tau \sum_i^N \alpha_i (\langle \psi(\Theta_{n+1}) | \psi(\Theta_n) \rangle \langle \psi(\Theta_n) | \mathbf{P}_i | \psi(\Theta_{n+1}) \rangle) + c.c.)$$
$$+ \tau^2 \sum_{i,j}^{N,N} \alpha_i \alpha_j \langle \psi(\Theta_n) | \mathbf{P}_j | \psi(\Theta_{n+1}) \rangle \langle \psi(\Theta_{n+1}) | \mathbf{P}_i | \psi(\Theta_n) \rangle \quad (7)$$

IMPLEMENTATION ON A QUANTUM COMPUTER

In our hybrid setup each term of eq 7 will be calculated separately by performing Hadamard tests, to extract the real and imaginary parts of $\langle \psi(\Theta_x) | \mathbf{U} | \psi(\Theta_y) \rangle = (a_{U,x,y} + i \times b_{U,x,y})$. $a_{U,x,y}$ and $b_{U,x,y}$ are real numbers. Important for the application on current noisy quantum hardware, the Hadamard test requires just one additional ancilla qubit, and only the ancilla qubit needs to be measured (see also Figure 1c). To implement the Hadamard test, the PQC to create the state must be embedded into $\mathbf{U}$ by $\mathbf{U}_{P,x,y} = \mathbf{U}_{\Theta_x}^\dagger P_i \mathbf{U}_{\Theta_y}$ (please keep in mind, the product of two unitary matrices results in a unitary matrix). When working with the truncated first order Taylor expansion, the following real and imaginary values from the Hadamard test are required: $\langle + | \mathbf{U}_{\Theta_{n+1}}^\dagger \mathbf{U}_{\Theta_n} | + \rangle$ and $\langle + | \mathbf{U}_{\Theta_{n+1}}^\dagger \mathbf{P}_i \mathbf{U}_{\Theta_n} | + \rangle$, for every Pauli operator P_i in $\mathbf{H} = \sum_i^N \alpha_i \mathbf{P}_i$. Afterward, the entire cost function is pieced together on a classical computer, demonstrating the parallel nature of this ansatz (the same argument holds for VQE[16]):

$$\left| \langle \psi(\Theta_{n+1}) | \left(1 - \tau \sum_i^N \alpha_i \mathbf{P}_i\right) | \psi(\Theta_n) \rangle \right|^2$$
$$= \left| \langle + | \mathbf{U}_{\Theta_{n+1}}^\dagger \left(1 - \tau \sum_i^N \alpha_i \mathbf{P}_i\right) \mathbf{U}_{\Theta_n} | + \rangle \right|^2$$
$$= [1 + (a_{1,n,n+1} + ib_{1,n,n+1})(a_{1,n+1,n} + ib_{1,n+1,n})]/2$$
$$- \tau \sum_i^N [\alpha_i (a_{1,n,n+1} + ib_{1,n,n+1})(a_{P_i,n+1,n} + ib_{P_i,n+1,n})]$$
$$- \tau \sum_i^N [\alpha_i (a_{1,n+1,n} + ib_{1,n+1,n})(a_{P_i^\dagger,n,n+1} + ib_{P_i^\dagger,n,n+1})]$$
$$+ \tau^2 \sum_{i,j}^{N,N} [\alpha_i \alpha_j (a_{P_i^\dagger,n,n+1} + ib_{P_i^\dagger,n,n+1})(a_{P_j,n+1,n} + ib_{P_j,n+1,n})] \quad (8)$$

As $\langle + | \mathbf{U}_{\Theta_{n+1}}^\dagger \mathbf{P}_i \mathbf{U}_{\Theta_n} | + \rangle$ is the complex conjugate of $\langle + | \mathbf{U}_{\Theta_n}^\dagger \mathbf{P}_i^\dagger \mathbf{U}_{\Theta_{n+1}} | + \rangle$ with $b_{P_i,n+1,n} = -b_{P_i^\dagger,n,n+1}$ and $a_{P_i,n+1,n} = a_{P_i^\dagger,n,n+1}$, eq 8 can be simplified to

$$\left| \langle \psi(\Theta_{n+1}) | \left(1 - \tau \sum_i^N \alpha_i \mathbf{P}_i\right) | \psi(\Theta_n) \rangle \right|^2$$
$$= \left| \langle + | \mathbf{U}_{\Theta_{n+1}}^\dagger \left(1 - \tau \sum_i^N \alpha_i \mathbf{P}_i\right) \mathbf{U}_{\Theta_n} | + \rangle \right|^2$$
$$= [1 + (a_{1,n+1,n} - ib_{1,n+1,n})(a_{1,n+1,n} + ib_{1,n+1,n})]/2$$
$$- \tau \sum_i^N [\alpha_i (a_{1,n+1,n} - ib_{1,n+1,n})(a_{P_i,n+1,n} + ib_{P_i,n+1,n})]$$
$$- \tau \sum_i^N [\alpha_i (a_{1,n+1,n} + ib_{1,n+1,n})(a_{P_i,n+1,n} - ib_{P_i,n+1,n})]$$
$$+ \tau^2 \sum_{i,j}^{N,N} [\alpha_i \alpha_j (a_{P_i,n,n+1} - ib_{P_i,n,n+1})(a_{P_j,n+1,n} + ib_{P_j,n+1,n})] \quad (9)$$

Now the classical optimizer maximizes the real part of eq 9. Additionally, it enforces that the linear decomposition of $|\langle \psi(\Theta_{n+1}) | (1 - \tau \sum_i^N \alpha_i \mathbf{P}_i) | \psi(\Theta_n) \rangle|^2$ has no imaginary component. The advantage of this technique, by choosing a reasonable small τ, is that the difference between Θ_n and Θ_{n+1} can be controlled.

RESULTS AND DISCUSSION

Figure 2a shows the imaginary time evolution for LiH at a distance of 0.8 Å. A highly trivial ansatz circuit has been used with six $x/y/z$ rotations per qubit. A parity mapper was used for the Fermion-to-qubit conversion, and the basis set is STO-3G leading to 10 qubits. The optimization is based on the COBYLA algorithm with 1000 iterations. Further details are specified in the Methods section. A smaller τ directly results in a slower progression toward the ground state, but fewer optimization iterations are needed to find the next set of rotational angles (Figure 2a). We have evaluated the average absolute difference of the rotational angles for the first 20 time steps. It increases from 0.009 to 0.019 and reaches 0.023 for $\tau = 0.01$, $\tau = 0.1$, and $\tau = 1$, respectively. So there is a trade-off which can be fine-tuned depending on the molecule of interest.
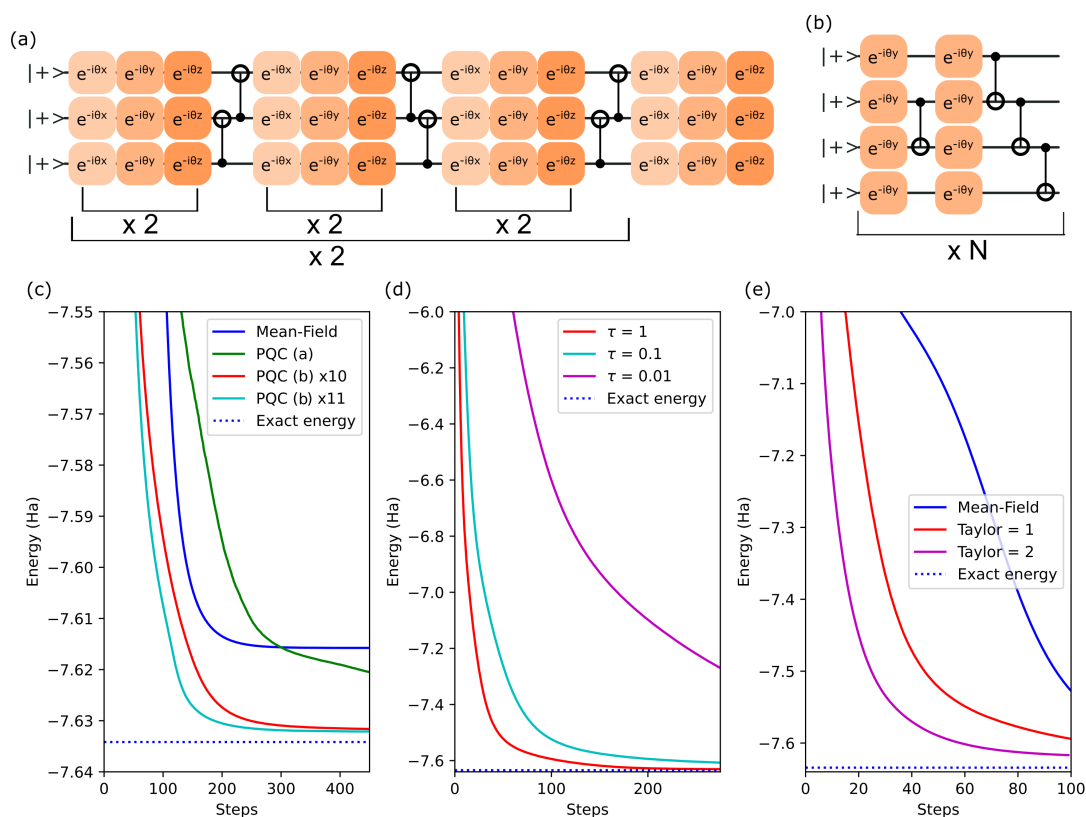
Figure 3. Imaginary time-evolution trajectories (c) are computed for two different PQCs with entanglements (a) and (b). (d) ITE of circuit (b) with $N = 10$ for three different τ. Mean-Field corresponds to the PQC shown in Figure 1a with 6 layers. (e) Influence of a higher Taylor order for circuit (b) with $N = 10$.

On the other hand, we find that the progression toward the ground state increases when taking higher orders of the Taylor expansion into account (see eq 4). The faster convergence can be seen in Figure 2b. The number of Pauli operators to compute grows exponentially with the Taylor order, e.g., for LiH 398793 elements (second order) instead of 632 elements (first order). The complexity of each quantum circuits stays the same. The higher number of Pauli gates per quantum circuit (in the case of second order expansion: $P_i \times P_j$ instead of P_i), can be simplified with the product rule for Pauli operators: $\sigma_i \sigma_j = \delta_{ij} 1 + i \sum_{k \in x,y,z} \epsilon_{ijk} \sigma_k$.

**Parameterized Quantum Circuits with Entanglement.** So far we did not consider any gates within the PQC which would lead to entanglement. To study ITE beyond the mean-field ansatz,[37] additional c-not gates are added. Figure 3a,b shows two possible circuits which have been used to compute the ground state with the help of ITE. In all three cases the quality of the solution is improved as the ITE converges toward a state with lower energy (see Figure 3c), and in the case of the PQC shown in Figure 3b even fewer time-steps are necessary. Similar to the computation shown in Figure 2a, a smaller τ leads to a slower progression toward the ground state (Figure 3d). We would expect that computations with smaller τ are more resilient with respect to errors. Considering a higher Taylor order, on the other hand, leads to a faster progression toward the ground state (Figure 3e).

When directly maximizing the overlap between parametrized circuit and the ground state $(|\langle \psi(\Theta)|\psi_{GS}\rangle|^2)$, a fidelity of 0.99973 is reached for the 10-layer circuit shown in Figure 3b. The corresponding energy of -7.63338 Ha is close to -7.63417

Ha, the energy of the ground state. Without entanglement the lowest energy state computed is located at -7.61577 Ha with a fidelity of 0.98162 (six layers of the PQC from Figure 1a). This shows that the additional gates to create entanglement in the PQC of Figure 3 improve the quality of the ground state computation. The price for the improved precision is a more complex quantum-circuit. By using the Hadamard test to compute the real and imaginary parts of the cost function, each c-not gate is implemented as a three-qubit gate (see Figure 1c).

Experimental Results. Finally, we have used the IBM-Q network to run our algorithm on a real quantum computer. Because of the limited computational resources we are restricted to focus on molecular hydrogen at the chemically less favorable distance of 0.074 Å. As for LiH, the Hamiltonian (STO-3G) is built with the help of IBM's Qiskit.[38] A parity mapper is used for the Fermion-to-qubit transformation, and the electronic structure of H_2 is described with two qubits (see Methods section for more details). We want to highlight that our PQC to describe the ground state consists of only one set of x, y, z rotation for each qubit. As a benchmark we have used the same ansatz circuit for the variational eigensolver package of IBM's Qiskit.[38] This allowed us to test the feasibility of our algorithm.

The experimental results are summarized in Figure 4, which shows the energy as a function of time-evolution/calculation steps. Interestingly, we note that, in simulation as well as on the actual hardware, a step decrease of the energy of the time-evolved hydrogen molecule is observed. Because of the limited access to quantum hardware, we want to stress that these experiments might not be representative. Nevertheless, they are in good agreement with simulations. Therefore, we believe ITE's
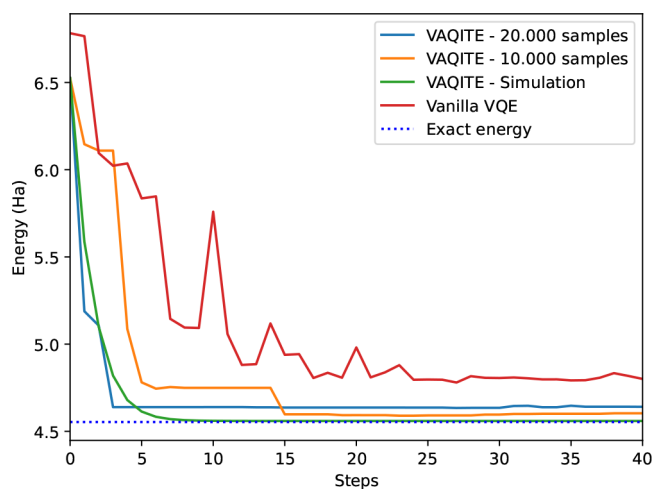
Figure 4. Ground state calculation of H_2 via simulation and on an IBM-Q quantum computer.

exponential suppression of excited states is of advantage when calculating ground state energies. But, in contrast to VQE, our algorithm is based on the Hadamard test and requires controlled unitary operations: In this case, not only the Hamiltonian but also of the parametrized ansatz circuit. In return, only one qubit needs to be measured. But the controlled operations (i.e., c-not gates) are still difficult to implement on NISQ quantum computers. In agreement with literature,[39] we also notice that the error rate increases with the total number of c-not operations per quantum circuit. We have addressed this by using mapomatic to find the best low noise subgraph on the target quantum systems for a certain quantum circuit.[40] This has strongly improved the results, as no convergence was detected without prior circuit mapping.

According to the Qiskit log file, the total computational time on a quantum computer (mostly IBMQ Mumbai) was roughly 60 h, not counting the classical calculations, which are in comparison negligible. However, the ground state was reached already after 6 time-evolution steps, corresponding to 7 h of measurements on a quantum computer. The computational time can be reduced further by choosing a lower sample count, which is with 10000 or even 20000 much too high.

CONCLUSION

To summarize, we have shown how ITE can be conducted with the help of a Taylor expansion series and a Hadamard test. For this hybrid algorithm, the quantum computer is used as a coprocessor. Time evolution is conducted in an iterative manner and the decomposition of the Hamiltonian allows us to calculate each term individually. But the number of terms of the cost function increases quickly with the size of the molecule. While the decomposed Hamiltonian of H_2 consists of 5 elements, LiH already has ~600, O_2 of roughly 15000, and O_3 more than 30000. When working with the expectation values, it has been shown that, by grouping the Pauli strings efficiently, the number of operators can be reduced heavily.[41] In the case of LiH from roughly 600 down to 130. Additionally, there are ideas how to rate the importance of the Pauli strings with respect to the gradient of the cost function: Terms with little importance are either dropped[42] or merged.[43] In the future, causal cones might help to reduce the qubit count of our PQC,[44,45] so that only a fraction of the circuit describing the molecular state needs to be computed. The remaining qubits can be used to implement error

mitigation techniques, e.g., symmetry verification, to increase the robustness of this algorithm.[46]

METHODS

The calculations are implemented with the help of IBM's Qiskit 0.21.0.[38] Their parity mapper is used for the Fermion-to-qubit transformation, and the Hamiltonian is expressed as a sum of Pauli-strings $\mathbf{H} = \sum_i^N \alpha_i \mathbf{P}_i$ (again by using Qiskit). The used basis set is STO-3G[47] for LiH as well as H_2. For the results presented in this work, we have computed the real and imaginary parts of $\langle +|\mathbf{U}_{\Theta_{n+1}}^\dagger \mathbf{P}_i \mathbf{U}_{\Theta_n}|+\rangle$ to build the cost function as shown in eq 9. For the sake of performance, a state vector ansatz was used for Figures 2 and 3 to compute the real and imaginary components of the cost function. Figure 4, on the other hand, was computed on an actual quantum computer, and only the Hadamard test, as sketched in Figure 1c, was executed to extract the real and imaginary values. Here, the quantum-circuit has been optimized for the actual quantum device by using mapomatic to find the best low noise subgraph on the target quantum system.[40] The used quantum-computer was mostly IBMQ Mumbai with 27 qubits in total. The optimization was done by using the constrained optimization by linear approximation algorithm[48,49] as implemented in SciPy[50] with 1000 (Figure 2), 4000 (Figure 3), and 100 (Figure 4) iterations, respectively. Classically, the ground state was computed by using Numpy as a benchmark.[51]

AUTHOR INFORMATION

Corresponding Author

Matthias Koch — *Applied Mathematics, Bayer AG, 51368 Leverkusen, Germany;* ● orcid.org/0009-0005-9479-3156; Email: matthias.koch2@bayer.com

Authors

Oliver Schaudt — *Applied Mathematics, Bayer AG, 51368 Leverkusen, Germany*
Georg Mogk — *Applied Mathematics, Bayer AG, 51368 Leverkusen, Germany*
Thomas Mrziglod — *Applied Mathematics, Bayer AG, 51368 Leverkusen, Germany*
Helmut Berg — *Enabling Technologies, Bayer AG, 51368 Leverkusen, Germany*
Michael Edmund Beck — *R&D, Crop Science, Bayer AG, 40789 Monheim, Germany;* ● orcid.org/0000-0001-9095-3881

Complete contact information is available at:
https://pubs.acs.org/10.1021/acsomega.3c01060

Notes
The authors declare no competing financial interest.

ACKNOWLEDGMENTS

REFERENCES
(1) Macalino, S. J. Y.; Gosu, V.; Hong, S.; Choi, S. Role of computer-aided drug design in modern drug discovery. *Archives of pharmacal research* **2015**, *38*, 1686−1701.
(2) Kapetanovic, I.M. Computer-aided drug discovery and development (CADDD): in silico-chemico-biological approach. *Chemico-biological interactions* **2008**, *171*, 165−176.
(3) Hillisch, A.; Heinrich, N.; Wild, H. Computational chemistry in the pharmaceutical industry: from childhood to adolescence. *ChemMedChem.* **2015**, *10*, 1958−1962.

(4) Deglmann, P.; Schafer, A.; Lennartz, C. Application of quantum calculations in the chemical industry - An overview. *Int. J. Quantum Chem.* **2015**, *115*, 107−136.

(5) Raghavachari, K.; Anderson, J. B. Electron correlation effects in molecules. *J. Phys. Chem.* **1996**, *100*, 12960−12973.

(6) Jorgensen, W. L. The many roles of computation in drug discovery. *Science* **2004**, *303*, 1813−1818.

(7) Sliwoski, G.; Kothiwale, S.; Meiler, J.; Lowe, E. W. Computational methods in drug discovery. *Pharmacol. Rev.* **2014**, *66*, 334−395.

(8) Leelananda, S. P; Lindert, S. Computational methods in drug discovery. *Beilstein journal of organic chemistry* **2016**, *12*, 2694−2718.

(9) Cournia, Z.; Allen, B.; Sherman, W. Relative binding free energy calculations in drug discovery: recent advances and practical considerations. *J. Chem. Inf. Model.* **2017**, *57*, 2911−2937.

(10) Aspuru-Guzik, A.; Dutoi, A. D.; Love, P. J.; Head-Gordon, M. Simulated quantum computation of molecular energies. *Science* **2005**, *309*, 1704−1707.

(11) Lloyd, S. Universal quantum simulators. *Science* **1996**, *273*, 1073−1078.

(12) Lanyon, B. P.; Whitfield, J. D.; Gillett, G. G.; Goggin, M. E.; Almeida, M. P.; Kassal, I.; Biamonte, J. D.; Mohseni, M.; Powell, B. J.; Barbieri, M.; et al. Towards quantum chemistry on a quantum computer. *Nature Chem.* **2010**, *2*, 106−111.

(13) Fowler, A. G.; Mariantoni, M.; Martinis, J. M.; Cleland, A. N. Surface codes: Towards practical large-scale quantum computation. *Phys. Rev. A* **2012**, *86*, 032324.

(14) Chen, Z.; Satzinger, K. J.; Atalaya, J.; Korotkov, A. N.; Dunsworth, A.; Sank, D.; Quintana, C.; McEwen, M.; Barends, R.; Klimov, P. V.; et al. Exponential suppression of bit or phase errors with cyclic error correction. *Nature* **2021**, *595*, 383.

(15) Endo, S.; Cai, Z.; Benjamin, S. C.; Yuan, X. Hybrid quantum-classical algorithms and quantum error mitigation. *J. Phys. Soc. Jpn.* **2021**, *90*, 032001.

(16) Peruzzo, A.; McClean, J.; Shadbolt, P.; Yung, M.-H.; Zhou, X.-Q.; Love, P. J.; Aspuru-Guzik, A.; O'Brien, J. L. A variational eigenvalue solver on a photonic quantum processor. *Nat. Commun.* **2014**, *5*, 4213.

(17) Kandala, A.; Mezzacapo, A.; Temme, K.; Takita, M.; Brink, M.; Chow, J. M.; Gambetta, J. M. Hardware-efficient variational quantum eigensolver for small molecules and quantum magnets. *Nature* **2017**, *549*, 242−246.

(18) Moll, N.; Barkoutsos, P.; Bishop, L. S; Chow, J. M; Cross, A.; Egger, D. J; Filipp, S.; Fuhrer, A.; Gambetta, J. M; Ganzhorn, M.; et al. Quantum optimization using variational algorithms on near-term quantum devices. *Quantum Science and Technology* **2018**, *3*, 030503.

(19) Cerezo, M.; Arrasmith, A.; Babbush, R.; Benjamin, S. C.; Endo, S.; Fujii, K.; McClean, J. R.; Mitarai, K.; Yuan, X.; Cincio, L.; et al. Variational quantum algorithms. *Nature Reviews Physics* **2021**, *3*, 625−644.

(20) Wecker, D.; Hastings, M. B.; Troyer, M. Progress towards practical quantum variational algorithms. *Phys. Rev. A* **2015**, *92*, 042303.

(21) McClean, J. R.; Boixo, S.; Smelyanskiy, V. N.; Babbush, R.; Neven, H. Barren plateaus in quantum neural network training landscapes. *Nat. Commun.* **2018**, *9*, 4213.

(22) Goldberg, A.; Schwartz, J. L Integration of the Schrödinger equation in imaginary time. *J. Comput. Phys.* **1967**, *1*, 433−447.

(23) Bader, P.; Blanes, S.; Casas, F. Solving the Schrödinger eigenvalue problem by the imaginary time propagation technique using splitting methods with complex coefficients. *J. Chem. Phys.* **2013**, *139*, 124117.

(24) McArdle, S.; Jones, T.; Endo, S.; Li, Y.; Benjamin, S. C.; Yuan, X. Variational ansatz-based quantum simulation of imaginary time evolution. *npj Quantum Information* **2019**, *5*, 75.

(25) Cleland, D.; Booth, G. H.; Alavi, A. Communications: Survival of the fittest: Accelerating convergence in full configuration-interaction quantum Monte Carlo. *J. Chem. Phys.* **2010**, *132*, 041103.

(26) Booth, G. H.; Thom, A. J. W.; Alavi, A. Fermion Monte Carlo without fixed nodes: A game of life, death, and annihilation in Slater determinant space. *J. Chem. Phys.* **2009**, *131*, 054106.

(27) Yang, Y.; Lu, B.-N.; Li, Y. Accelerated quantum Monte Carlo with mitigated error on noisy quantum computer. *PRX Quantum* **2021**, *2*, 040361.

(28) Huggins, W. J.; O'Gorman, B. A.; Rubin, N. C.; Reichman, D. R.; Babbush, R.; Lee, J. Unbiasing fermionic quantum Monte Carlo with a quantum computer. *Nature* **2022**, *603*, 416−420.

(29) Liu, T.; Liu, J.-G.; Fan, H. Probabilistic nonunitary gate in imaginary time evolution. *Quantum Information Processing* **2021**, *20*, 204.

(30) Motta, M.; Sun, C.; Tan, A. T. K.; O'Rourke, M. J.; Ye, E.; Minnich, A. J.; Brandao, F. G. S. L.; Chan, G. K.-L. Determining eigenstates and thermal states on a quantum computer using quantum imaginary time evolution. *Nat. Phys.* **2020**, *16*, 205−210.

(31) Grover, L. K. A fast quantum mechanical algorithm for database search. *STOC '96: Proceedings of the twenty-eighth annual ACM symposium on Theory of Computing*; Association for Computing Machinery: 1996; pp 212−219.

(32) Grover, L. K. Quantum mechanics helps in searching for a needle in a haystack. *Physical review letters* **1997**, *79*, 325.

(33) Lin, S.-H.; Dilip, R.; Green, A. G.; Smith, A.; Pollmann, F. Real-and imaginary-time evolution with compressed quantum circuits. *PRX Quantum* **2021**, *2*, 010342.

(34) Seeley, J. T.; Richard, M. J.; Love, P. J. The Bravyi-Kitaev transformation for quantum computation of electronic structure. *J. Chem. Phys.* **2012**, *137*, 224109.

(35) Jordan, P.; Wigner, E. Über das paulische äquivalenzverbot. *Z. Phys.* **1928**, *47*, 631.

(36) Bravyi, S. B.; Kitaev, A. Y. Fermionic quantum computation. *Annals of Physics* **2002**, *298*, 210−226.

(37) Ryabinkin, I. G.; Genin, S. N.; Izmaylov, A. F. Relation between fermionic and qubit mean fields in the electronic structure problem. *J. Chem. Phys.* **2018**, *149*, 214105.

(38) Sajid Anis, M. D.; et al. *Qiskit: An Open-source Framework for Quantum Computing*; 2021; DOI: 10.5281/zenodo.2573505.

(39) Koch, D.; Martin, B.; Patel, S.; Wessing, L.; Alsing, P. M. Demonstrating NISQ era challenges in algorithm design on IBMas 20 qubit quantum computer. *AIP Advances* **2020**, *10*, 095101.

(40) Nation, P. D.; Treinish, M. Suppressing Quantum Circuit Errors Due to System Variability. *PRX Quantum* **2023**, *4*, 010327.

(41) Hamamura, I.; Imamichi, T. Efficient evaluation of quantum observables using entangled measurements. *npj Quantum Information* **2020**, *6*, 56.

(42) Grimsley, H. R.; Economou, S. E.; Barnes, E.; Mayhall, N. J. An adaptive variational algorithm for exact molecular simulations on a quantum computer. *Nat. Commun.* **2019**, *10*, 3007.

(43) Gomes, N.; Zhang, F.; Berthusen, N. F.; Wang, C.-Z.; Ho, K.-M.; Orth, P. P.; Yao, Y. Efficient step-merged quantum imaginary time evolution algorithm for quantum chemistry. *J. Chem. Theory Comput.* **2020**, *16*, 6256−6266.

(44) Vidal, G. Class of quantum many-body states that can be efficiently simulated. *Physical review letters* **2008**, *101*, 110501.

(45) Benedetti, M.; Fiorentini, M.; Lubasch, M. Hardware-efficient variational quantum algorithms for time evolution. *Physical Review Research* **2021**, *3*, 033083.

(46) Bonet-Monroig, X.; Sagastizabal, R.; Singh, M.; O'Brien, T. E. Low-cost error mitigation by symmetry verification. *Phys. Rev. A* **2018**, *98*, 062339.

(47) Hehre, W. J.; Stewart, R. F.; Pople, J. A. Self-consistent molecular-orbital methods. I. Use of Gaussian expansions of Slater-type atomic orbitals. *J. Chem. Phys.* **1969**, *51*, 2657−2664.

(48) Powell, M. J. D. *A direct search optimization method that models the objective and constraint functions by linear interpolation*; Springer: 1994.

(49) Powell, M. J. D. A view of algorithms for optimization without derivatives. *Mathematics Today-Bulletin of the Institute of Mathematics and its Applications* **2007**, *43.5*, 170−174.

(50) Virtanen, P.; Gommers, R.; Oliphant, T. E.; Haberland, M.; Reddy, T.; Cournapeau, D.; Burovski, E.; Peterson, P.; Weckesser, W.; Bright, J.; et al. SciPy 1.0: Fundamental Algorithms for Scientific Computing in Python. *Nat. Methods* **2020**, *17*, 261−272.

(51) Harris, C. R.; Millman, K. J.; van der Walt, S. J.; Gommers, R.; Virtanen, P.; Cournapeau, D.; Wieser, E.; Taylor, J.; Berg, S.; Smith, N. J.; et al. Array programming with NumPy. *Nature* **2020**, *585*, 357−362.